

# Micro-sized Graphene-Based UWB Annular Ring Patch Antenna for Short-Range High-Speed Terahertz Wireless Systems



Asma Khabba, Jamal Amadid, Zakaria El Ouadi, Layla Wakrim, Saida Ibnyaich, Ahmed Jamal Abdullah Al-Gburi, and Abdelouhab Zeroual

**Abstract** Owing to the fascinating features of graphene material, graphene-based patch antennas have quickly attracted attentions in communication technologies for high-speed data transfer in terahertz band. Herein, we present in this chapter a careful study of a new ultra-wide band (UWB) graphene-based plasmonic terahertz (THz) antenna operating in the range of 7.4–8.4 THz, with a huge bandwidth of 1000 GHz. The resonant part of the antenna consists of a modified circular ring patch, designed on 2.4  $\mu\text{m}$ -thick silicon laminate with a high permittivity of 11.9. The resonating frequencies and the antenna operation band can be controllable by adjusting the graphene layers' chemical potential, where the desired UWB behavior is attained with a chemical potential of 2 eV. The suggested antenna possesses a super compact geometry of  $24 \times 24 \mu\text{m}$  along with attractive radiation behavior in terms of gain (up to 5.5 dB) radiation efficiency (>97%). In addition, a high impedance matching is achieved which contributes in very low reflection coefficient of  $-53.5 \text{ dB}$ . According to the outcomes realized, it can be inferred that the proffered THz antenna would be an excellent solution for various applications in terahertz regime, including the explosive detection, material characterization, homeland defense, security scanning, biomedical imaging, sensing, video rate imaging system and the upcoming short-range high-speed wireless indoor communications.

**Keywords** Graphene · Terahertz · UWB · Antenna · Plasmonic · Indoor communication · High speed

---

A. Khabba (✉) · J. Amadid · Z. E. Ouadi · S. Ibnyaich · A. Zeroual  
Instrumentation, Signals and Physical Systems (I2SP) Team, Faculty of Sciences Semlalia, Cadi Ayyad University, Marrakesh, Morocco  
e-mail: [asma.khabba@edu.uca.ac.ma](mailto:asma.khabba@edu.uca.ac.ma)

L. Wakrim  
Laboratory of Innovation in Management and Engineering for Business (LIMIE), Higher Institute of Engineering and Business (ISGA), Marrakesh, Morocco

A. J. A. Al-Gburi  
Department of Electronic and Computer Engineering (FKEKK), Center of Telecommunication Research and Innovation (CeTRI), Universiti Teknikal Malaysia Melaka (UTeM), Durian Tunggal, Malacca, Malaysia

## 1 Introduction

During the past few years, the revolutionary advancement in wireless communications technologies generated a real need to an inexhaustible frequency bandwidth to fulfill the requirements of channel capacity, colossal data traffic rate, and uninterrupted connectivity [1–6]. These needs have attracted the researchers' interests toward a new massive frequency band spectrum, namely terahertz (THz) band. The latter is an electromagnetic (EM) spectrum lying between millimeter wave and infrared regions and occupying the spectral band from 0.1 to 10 THz. The region of THz band has appeared as a key solution to achieve high speed, secure, highly reliable wireless communications and unprecedented advanced technologies [7, 8]. The THz band technologies are gaining a rapid development to support several high potential applications such as ultra-fast communication [9], medical diagnostic [10], explosive detection [11], chemical, viruses' detection [12], remote sensing [13], imaging system [14], material characterization [15] and spectroscopic detection [16]. Indeed, the terahertz spectrum are able to hold up all these data-hungry applications due to many benefits like the enormous available frequency band, improved anti-interference performance, low diffraction and high spectral resolution compared to millimeter wave (mm-Wave) spectrum. However, the severe atmospheric path attenuation constitutes a significant hurdles for the commercialization of THz wireless systems. Accordingly, developing a compact antenna with high efficient performance is of first concern to indemnify the wasted energy referred to the considerable path loss in THz regime [17]. The antenna is the key unit enabling the transmission of EM waves in THz wireless communication where its characteristics, including the compactness, the bandwidth, efficiency and gain, etc., affect directly the THz system performance. This will inherently raise several defiances to the experts of antenna community and usher in a new era in the realm of planar antenna technology. In the other side, graphene material arouses a considerable scientific attentiveness due to its exceptional mechanical and electrical traits. It is explored as miracle substance enabling the good exploitation of terahertz portion [18]. Accordingly, many existing works are focused on graphene to design different antennas structures for THz applications, for instance, in Ref. [19], a THz antenna with graphene material is proposed for multiband application at 1.73/2.6/4.01/4.72 THz. In Ref. [20], a photoconductive dipole antenna is designed using graphene layer and put in comparison with a photoconductive dipole antenna made with gold metal, where a high emitted spectrum is reached while using graphene. In Ref. [21], a graphene patch antenna with superstrate is suggested to operate at 7 THz with total bandwidth of 386 GHz. Another graphene-based antenna with narrow bandwidth of 25 GHz is reported in [22]. In Ref. [23], a conventional patch antenna is presented with a total bandwidth of 280 GHz at 0.72 THz. In Ref. [24], a rectangular path antenna is created at 0.67 THz with only 40 GHz of bandwidth. Similarly in Ref. [25], a modified patch antenna is modeled using graphene as radiating material to work at 0.62 THz. The photonic band gaps were implanted in the substrate, while a restricted bandwidth of 34.9 GHz is reached.

Taking into account the wide bandwidth requirement for high data rate transmission, the main objective of this research work is the development of a new THz antenna supporting the ultra-wide band operation while preserving a suitable radiation performance and extremely small dimensions. This purpose is successfully accomplished by developing a teeny circular ring antenna powered by a 50  $\Omega$  microstrip feed line and backed by a full ground plane. The conducting parts of the proposed antenna are made of graphene material, while silicon substrate is chosen to build the design.

The remaining of the paper is organized as follows: The next section is allowed to introduce the graphene material and modeling. Section 3 presents the proffered antenna geometry. The antenna evolution procedures is studied in Sect. 4. A careful parametric study is done in Sect. 5. Section 6 brings the main achieved results. A comparative study is taken place in Sect. 7. Finally, Sect. 8 summarizes the performed study.

## 2 Modeling of Graphene Material

Graphene is a staggering carbon-based material with spectacular optical, electrical and mechanical properties. It is considered the magic key to entering the terahertz world through its wide door. In addition, one of the most advantage of graphene is the capability to support the transmission of surface plasmon polaritons (SPPs) waves on its surface which can be employed for miniaturization process even for antennas or other applications [26]. Indeed, the graphene surface plasmon polaritons are highly tunable and marked by low consumption, ultra-fast carrier mobility and strong localization [27]. The SPPs propagation as well as the graphene resonance are heavily depending on its complex electrical conductivity, where the latter is mainly depends on the key parameters, namely relaxation time ( $\tau$ ) and chemical potential ( $\mu_c$ ), i.e., (Fermi energy). Hence, the chemical potential can be altered through chemical doping or by applying electrostatic gate bias [28]. For an infinitesimally thin graphene surface with random-phase approximation (RPA), the surface electric conductivity ( $\sigma_s$ ) can be represented mathematically with the assistance of Kubo Formula which is denoted by Eq. (1) [21, 29], where, Fermi Dirac distribution is denoted by  $fd(\varepsilon) = \left( e^{\frac{\varepsilon - \mu_c}{k_B T}} + 1 \right)$ , and the collision frequency is represented by  $\Gamma = 1/2\tau$ .

Furthermore, the graphene total conductivity ( $\sigma_g$ ) [30] can be obtained by summing the two conductivity parts, the first part is the intra-band conductivity ( $\sigma_{\text{intra}}$ ), while the second is the inter-band conductivity ( $\sigma_{\text{inter}}$ ). The intra-band conductivity controls the graphene characteristics in infrared region, where the approximated Eq. (2) is given by Dured model, where  $q$  is the electron charge, Boltzmann constant is denoted by  $k_B$ ,  $T$  is the effective carrier temperature in Kelvin, reduced Plank constant is given by  $\hbar = h/2\pi$  and  $\omega$  is the angular frequency of the incident wave. Damping constant is expressed as  $\Gamma_c = q \hbar v_F^2 / \mu \mu_c$ , where,

$\mu = 10^4 \text{m}^2 \cdot \text{V}^{-1} \cdot \text{s}^{-1}$  is the electron mobility and  $v_F^2 = 10^6 \text{m} \cdot \text{s}^{-1}$  is the Fermi velocity. The other conductivity part, i.e., the inter-band conductivity, is dominating at higher frequency spectrum and it is expressed by Eq. (3).

$$\sigma_s = j \frac{q^2(\omega - j2\Gamma)}{\pi h^2} \left[ \frac{1}{(\omega - j2\Gamma)^2} \int_0^\infty \varepsilon \left( \frac{\partial f d(\varepsilon) - \partial f d(-\varepsilon)}{\partial \varepsilon} \right) \partial \varepsilon - \int_0^\infty \frac{f d(-\varepsilon) - f d(\varepsilon)}{(\omega - j2\Gamma)^2 - 4\left(\frac{\varepsilon}{h}\right)^2} \partial \varepsilon \right] \quad (1)$$

$$\sigma_{\text{intra}} = j \frac{q^2 k_B T}{\pi h (h\omega + j2\Gamma_c)} \left[ \frac{\mu_c}{k_B T} + 2 \ln \left( e^{\frac{\mu_c}{k_B T}} + 1 \right) \right] \quad (2)$$

$$\sigma_{\text{inter}} = j \frac{q^2}{4\pi h} \ln \left[ \frac{2|\mu_c| - (h\omega + j\Gamma_c)}{2|\mu_c| + (h\omega + j\Gamma_c)} \right] \quad (3)$$

The graphene material can be roughly modeled using the FIT-based (Finite Integration Technique) electromagnetic software, namely CST microwave studio for optical applications and terahertz spectrum. Accordingly, Fig. 1a and b expose the real and imaginary parts of the of the simulated graphene conductivity for various values of chemical potential ( $\mu_c$ ) and relaxation time ( $\tau$ ), respectively.

As illustrated, it can be clearly observed that the conductivity behavior changes significantly when augmenting the chemical potential ( $\mu_c$ ) and relaxation time ( $\tau$ ), which leads to produce a strong resonance at higher frequency range. Indeed, with the increase of chemical potential ( $\mu_c$ ), the absorption cross section raises and the resonance shifts toward high frequencies, where the same goes for relaxation time ( $\tau$ ). Hence, to tune the antenna resonance at high terahertz frequency, the graphene characteristics are chosen in the following manner; chemical potential ( $\mu_c$ ) is fixed at 2 eV, for the relaxation time ( $\tau$ ) is specified at  $10^{-12}$  s and the temperature T is chosen at 300 K.

### 3 Geometry of the Proposed THz Antenna

The configuration of the proposed antenna structure is exposed in Fig. 2. The antenna geometry is wisely built of  $2.4 \mu\text{m}$ -thick silicon substrate with permittivity  $\varepsilon_r$  of 11.9, tangent loss of 0.00025 and full area ( $W_s \times L_s$ ) of  $24 \times 24 \mu\text{m}^2$ . The proposed layout consists of a radiating annular ring with outer radius  $r_1$  and inner radius  $r_2$  of  $6.5$  and  $5 \mu\text{m}$ , respectively, powered by a  $50 \Omega$  microstrip feed line of length  $L_f = 5.6 \mu\text{m}$  and width  $W_f = 1.5 \mu\text{m}$ . A rectangular strip of width  $W_1 = 1.7 \mu\text{m}$  and length  $L_1 = 1.42 \mu\text{m}$  is placed at the outer edge of the annular ring, in the opposite direction to the feeding line for bandwidth enhancement goal. A full ground plane is used to back the structure, where the antenna conductive parts are made using  $0.4 \mu\text{m}$ -thick graphene layer.

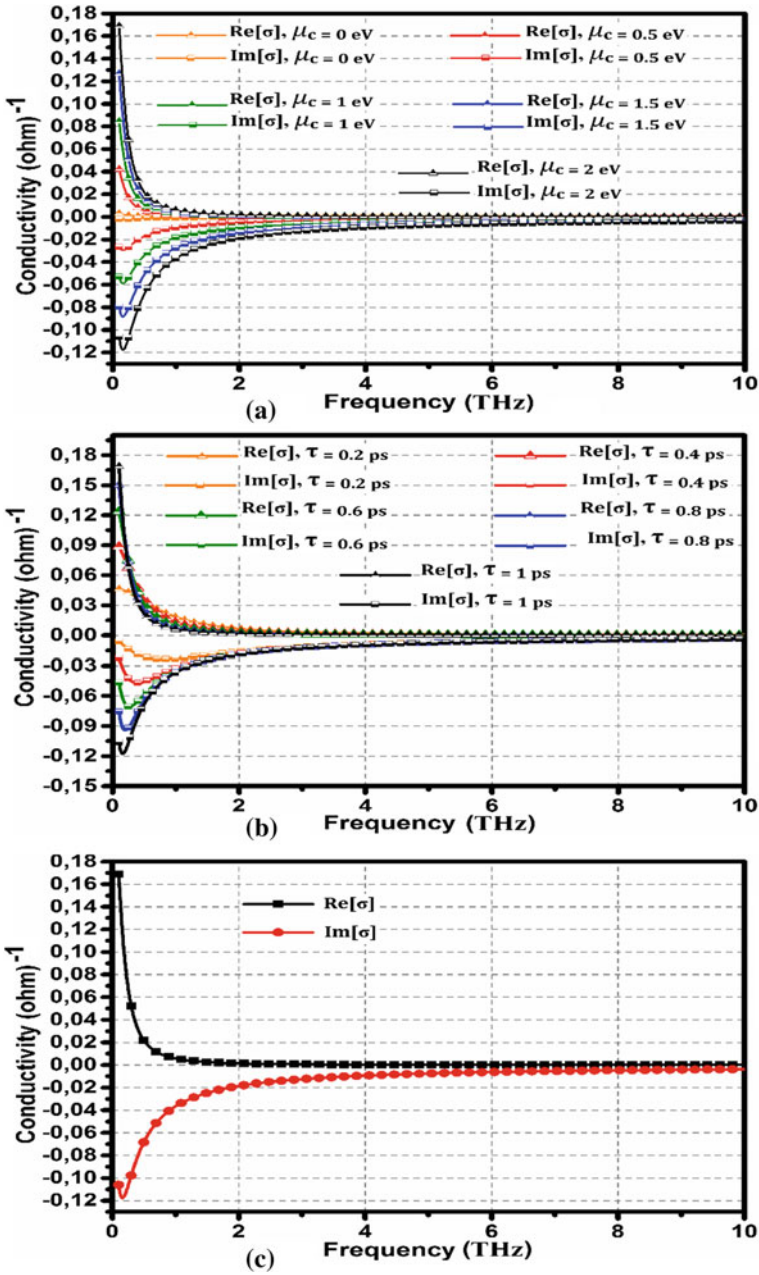
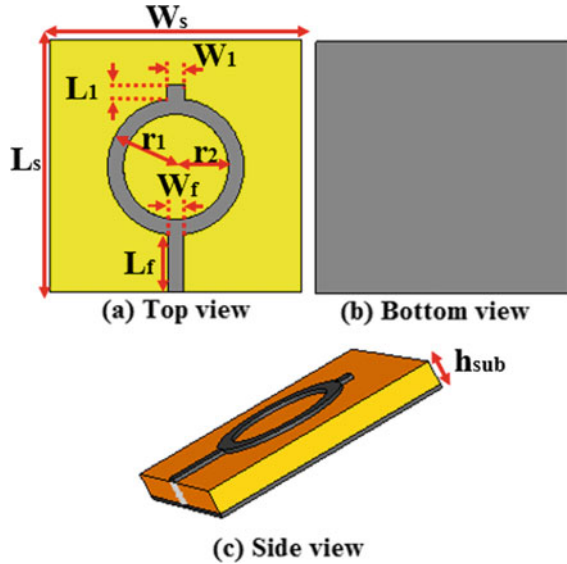


**Fig. 1** Conductivity variation with respect to **a** Chemical potential ( $\mu_c$ ), **b** relaxation time, **c** conductivity of proposed graphene with  $\mu_c = 2$  eV,  $\tau = 10^{-12}$  s and  $T = 300$  K

**Fig. 2** Layout of the graphene-based suggested antenna



A careful design construction and intense parameter optimization are made using the above mentioned software to reach the most-refined version of the suggested antenna providing the desirable operation. To find out the antenna design methodology, the next section investigates the antenna evolution procedure.

#### 4 Evolutionary Stages of the Suggested Antenna

In order to comprehend the operation principle of the proposed antenna design, Fig. 3 displays the essential evolution steps through which the final antenna geometry with the desired operation is reached. As clarified, the proposed antenna is the ameliorated version of the basic Circular Microstrip Patch Antenna (CMPA) developed over three essential steps, where the frequency response for all design steps is collected in Fig. 4. As demonstrated in Fig. 3a, the first step is accomplished by designing a conventional CMPA with complete ground plane, where the patch radius  $r_1$  is preliminary approximated using Eqs. (4–5). Then the overall dimensions refinement is done with the assistance of CST software to bring the antenna resonance in the band of interest. As perceived in Fig. 4, the conventional CMPA (Antenna-1) was firstly modeled to resonate around 8 THz frequency, however, the total bandwidth is only 177 GHz, while the impedance matching needs a considerable improvement. Hence, to extend the operating bandwidth and the impedance matching, geometrical modifications are required. Accordingly, in the second step exposed in Fig. 4, the basic CMPA is converted to an annular ring microstrip patch antenna (Antenna-2) by creating a circular slot with a radius  $r_2$  inside the resonant patch. As expected,

the reflection coefficient in Fig. 4 shows a great bandwidth enhancement from 177 to 720 GHz after adding the circular slot where a strong resonance is created at 8.11 THz. This is obtained through a fine refinement of the slot radius  $r_2$  which is fixed at  $5 \mu\text{m}$ , where the latter is approximately seventh wavelength ( $\frac{\lambda}{7}$ ) at 8.11 THz.

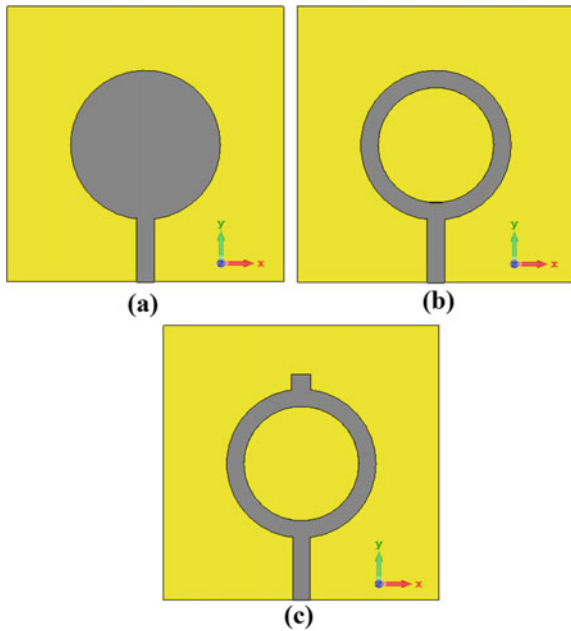
$$r_1 = \frac{F}{\left\{ 1 + \frac{2h_{\text{sub}}}{\pi \epsilon_r F} \left[ \ln\left(\frac{\pi F}{2h_{\text{sub}}}\right) + 1.7726 \right] \right\}^{1/2}} \tag{4}$$

$$F = \frac{8.791 \times 10^9}{f_r \sqrt{\epsilon_r}} \tag{5}$$

Hence, to well comprehend the circular slot effect, Fig. 5 shows the electric field distribution of the SPP before and after adding the slot. As configured, the etched slot has led to a strong confinement of the electric field propagation in the substrate inside the annular ring which enables the antenna to form its first resonance around 8.11 THz. Finally, as visualized in Fig. 3c, to get the coveted operation, a rectangular strip is inserted on the top edge of the annular ring which consequently contributes to reach the final design of the suggested antenna.

As can be seen in Fig. 4, the resonant strip engenders a new resonating frequency at 7.5 THz which bestowed further bandwidth-extension toward lower frequencies. The strip dimensions are properly tuned to extract the optimal antenna behavior

**Fig. 3** Stepwise design evolution, **a** Antenna-1 (Conventional antenna), **b** Antenna-2 (Ring antenna), **c** Proposed antenna



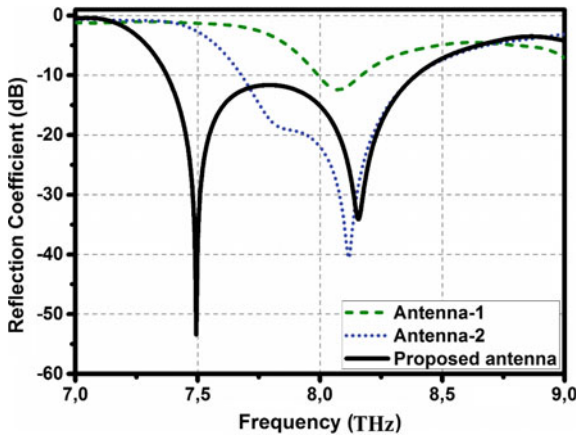


Fig. 4 Reflection coefficient of the evolutionary designs

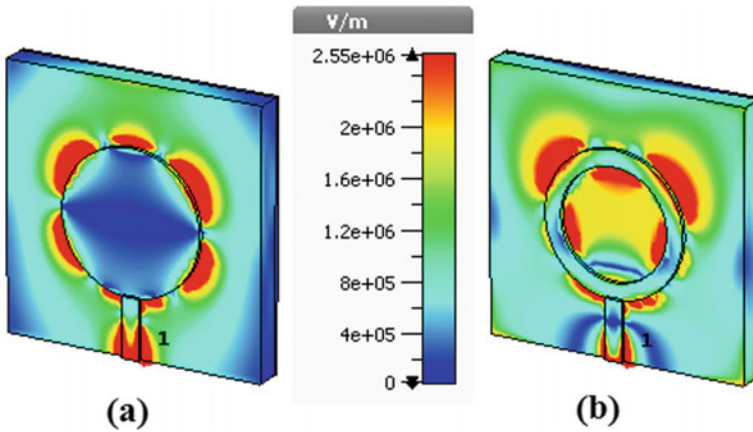


Fig. 5 SPP electric field distribution, a Antenna-1 at 8.07 THz, b Antenna-2 at 8.11 THz

where its effect can be easily glimpsed by observing the electric field pervasion in Fig. 6.

As described, a strong electric field intensity is surrounding the rectangular strip at 7.5 THz which indicates its main rule to generate the mentioned resonating frequency, whereas at 8.15 THz, the electric field propagation remains intense in the annular ring slot. So, to deeply analyze the effect of the antenna parameters on its operation behavior, an accurate parametric study is done in the next section.

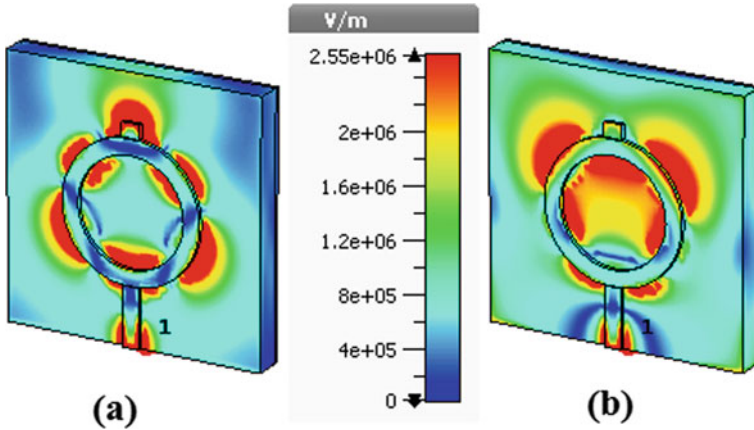


Fig. 6 SPP electric field distribution of the proposed antenna, a 7.5 THz, b 8.15 THz

### 5 Parametrical Analysis

Parametric analysis is an inevitable phase in antenna design to discover the optimal dimensions allowing the best antenna performance. Hence, this parametric analysis is performed with the intention to reveal the effect of the some basic parameters related to the annular ring and the rectangular strip on the antenna performance including the operating bandwidth, the impedance matching and the resonant frequencies. The influence of the inner radius  $r_2$ , the strip width  $W_1$  and length  $L_1$  is configured in Fig. 7. During the parametrical study, when altering a parameter, the other ones remain constant. As manifested in Fig. 7a, the reflection coefficient shows a hyper sensitivity and changes drastically when the inner radius  $r_2$  is increased from 3 to 6  $\mu\text{m}$ . Indeed, with  $r_2 = 3 \mu\text{m}$ , the antenna acts as multiband antenna with two resonant frequencies at 8.12 and 8.65 THz. The multiband operation converts to monoband operation around 8.21 THz when  $r_2$  is 4  $\mu\text{m}$ . The required operation is glimpsed when the inner radius  $r_2$  is 5  $\mu\text{m}$ , where the antenna bears an ultra-wide band of 1000 GHz and two resonant frequencies at 7.5 THz and 8.15 THz. However, when the inner radius  $r_2$  is augmented to 6  $\mu\text{m}$ , the impedance matching is distorted over the whole frequency range and inherently the operational bandwidth get lost. The effect of varying the rectangular strip width  $W_1$  is displayed in Fig. 7b. As shown, the slight variation of the parameter  $W_1$  from 1.3 to 1.9  $\mu\text{m}$  with a step of 0.1  $\mu\text{m}$  has a clear impact on the impedance matching of both resonating frequencies as well as the adjustment of the lower resonating frequency.

Indeed, it can be remarked that the latter is decreased from 7.59 to 7.5 THz when the width  $W_1$  increases from 1.3 to 1.7  $\mu\text{m}$  while it rising back to 7.53 THz when  $W_1$  is 1.9  $\mu\text{m}$ . The most suitable result is attained at  $W_1 = 1.7 \mu\text{m}$ . The outcome of swapping the strip length  $L_1$  is plotted if Fig. 7c.

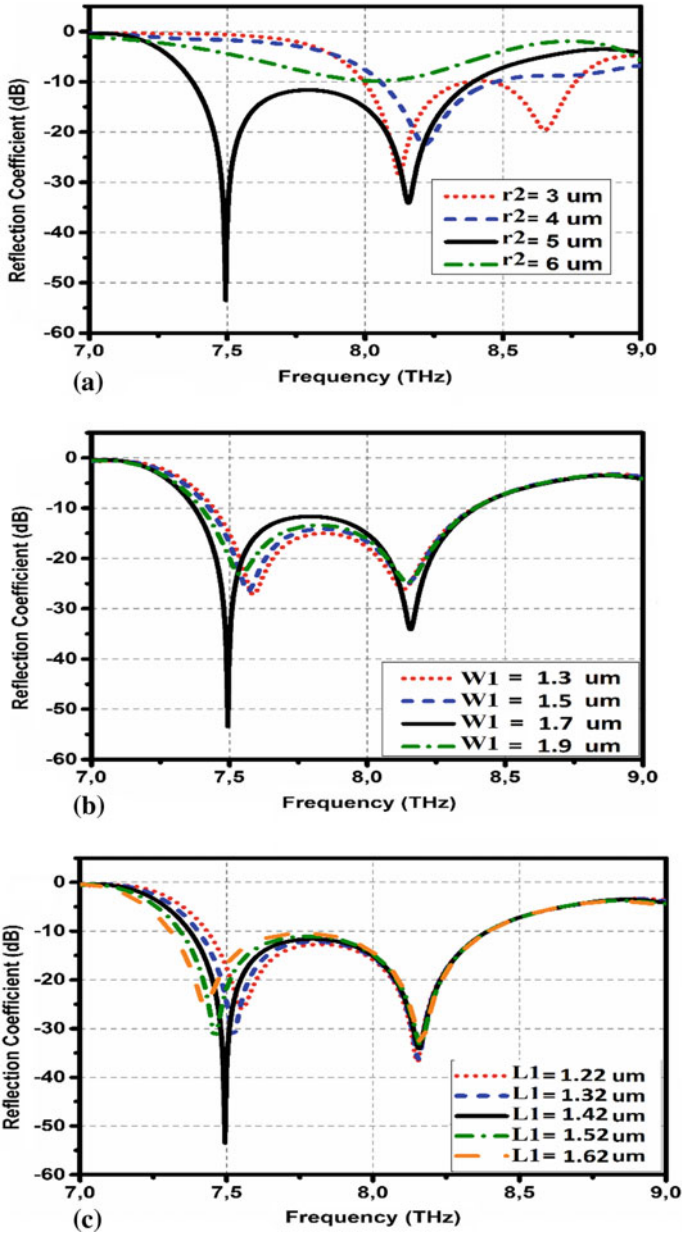


Fig. 7 Parametric analysis of the some key parameters, **a** inner radius  $r_2$ , **b** strip width  $W_1$ , **c** strip length  $L_1$

As exposed, the effect of altering the parameter  $L_1$  from 1.22 to 1.62  $\mu\text{m}$  has principally a direct influence on the lower resonance frequency and the impedance matching, while the higher resonance frequency value still unchanged. By increasing  $L_1$ , the first resonance shifts down from 7.55 to 7.42 THz, while the sought-after frequency response is acquired with  $L_1 = 1.42 \mu\text{m}$ . Consequently, the performed parametrical analysis assures the main role of the parameters, namely the inner radius  $r_2$ , the strip length  $L_1$  and width  $W_1$  to neatly control the reflection coefficient and adjust the resonant frequencies and operating bandwidth. In addition, they can properly amend the impedance matching to offer the best performance operation. After wisely analyzing the antenna parameters and describing their effect on the frequency response, the next section is dedicated to present the results and antenna performance.

## 6 Performance Results and Discussions

This section is allowed to present and describe the traits of the suggested antenna including the impedance and radiation characteristics.

### 6.1 Reflection Coefficient

As illustrated in Fig. 8, the suggested antenna bears an ultra-wide bandwidth of 1000 GHz from 7.4 to 8.4 THz with high impedance matching where the reflection coefficient at the first and second resonant frequencies reaches to  $-54 \text{ dB}$  and  $-34 \text{ dB}$ . The attained bandwidth could be used for various high-speed wireless applications in terahertz spectrum.

**Fig. 8** Reflection coefficient of the proposed antenna

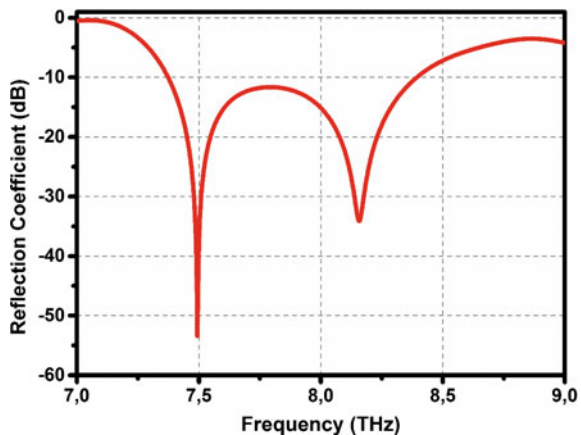
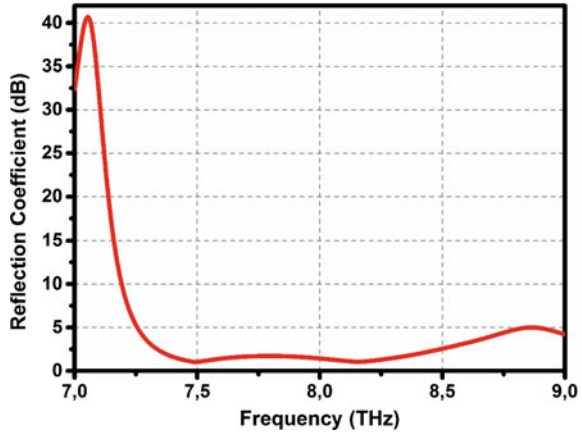


**Fig. 9** VSWR of the suggested antenna



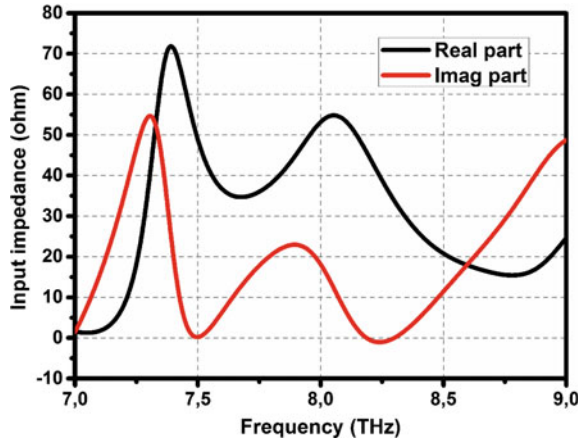
## 6.2 Voltage Standing Wave Ratio

As the reflection coefficient, the Voltage Standing Wave Ratio (VSWR) can be used to visualize the impedance bandwidth of the proposed antenna. Indeed, the operational bandwidth can be determined when the VSWR is below 2. Accordingly, same as the reflection coefficient, the plotted VSWR in Fig. 9 shows a large operating bandwidth from 7.4 to 8.4 THz at VSWR < 2 which in turn indicates a good agreement and validates the operating band.

## 6.3 Input Impedance

The antenna input impedance ( $Z_{in}$ ) is the voltage to current ratio at the input of the antenna. It is a complex number where the input resistance is the real part  $\text{Re}[Z_{in}]$ , while the imaginary part  $\text{Im}[Z_{in}]$  is the input reactance. To fulfill a high impedance matching at a given frequency which inherently means a highly radiated power, the input impedance should be close to  $50 \Omega$ . This signifies that the real part must be close to  $50 \Omega$ , while the imaginary part should be near to zero. In the ideal case, the imaginary part of the input impedance is null and the real part is exactly  $50 \Omega$  which indicates that the antenna receives and radiates the total incident power. The input impedance of the proposed antenna is configured in Fig. 10, as can be seen the antenna realizes a high impedance matching at both resonance frequencies, where the real and imaginary parts ( $\text{Re}[Z_{in}]$ ,  $\text{Im}[Z_{in}]$ ) at the lower and higher resonance frequencies are  $(50.02, 0.2) \Omega$  and  $(49.23, 1.8) \Omega$ , respectively.

**Fig. 10** Antenna input impedance



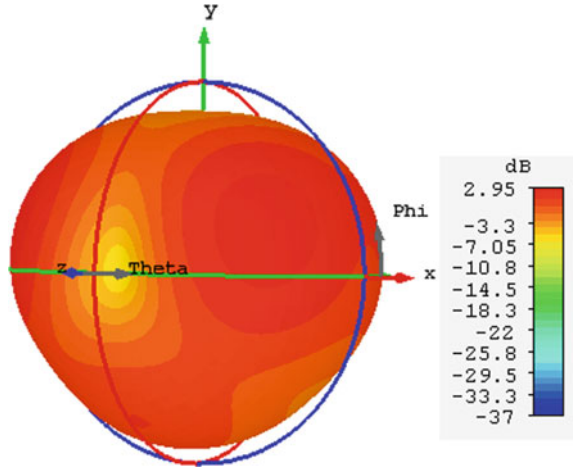
### 6.4 Radiation Patterns

The radiation pattern describes the variations of the radiated power in function of the direction away from the antenna. Hence, the three-dimensional radiation patterns 7.5, 7.8, 8 and 8.15 THz are plotted in Figs. 11, 12 and 13 and 14, respectively. In addition, the polar (2D) representation of the radiation pattern at the mentioned frequencies is illustrated in Figs. 15, 16, 17 and 18, respectively. As displayed, the 3D configuration assures a good and stable radiation behavior of the suggested antenna at all selected frequencies where the maximum gain achieved is 2.95, 3.57, 3.82 and 4.6 dB at 7.5 THz, 7.8 THz, 8 THz and 8.15 THz, respectively. Furthermore, the 2D radiation patterns at the above mentioned frequencies in the two cutting planes, i.e., H-plane ( $\phi = 0^\circ$ ) and E-plane ( $\phi = 90^\circ$ ) show for most frequencies a quasi-omnidirectional pattern in H-plane and bidirectional pattern in E-plane which demonstrates a uniform radiation. In the other side, the gain and radiation efficiency along the operating bandwidth are traced in Fig. 19. As displayed, the proposed design is marked by a good gain characteristic varying between 2.6 and 5 dB over the working band. In addition, an excellent radiation efficiency trait is remarked along the whole bandwidth where the minimum value is more than 97.5% and the maximum reached is up to 99.72%. After describing the achievements of the suggested antenna, a brief comparison with some existing work is reported in the next section to well evaluate the antenna performance.

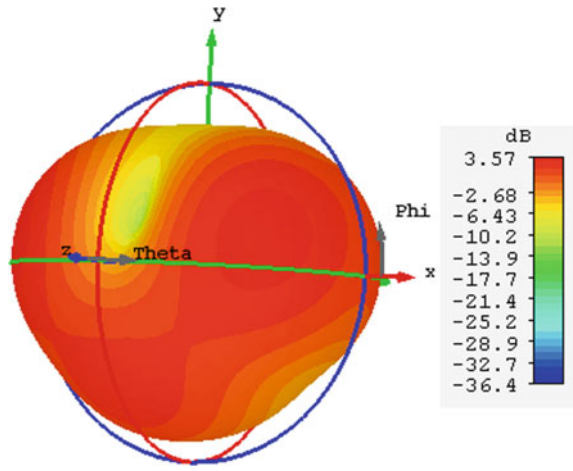
## 7 Comparison with Other Reported Work

Table 1 presents a comparative study of the proffered antenna performance with some other previous works. Certainly, many research are reported in the literature to propose different antenna design structure for the upcoming terahertz applications.

**Fig. 11** 3D radiation pattern at 7.5 THz



**Fig. 12** 3D radiation pattern at 7.8 THz



Indeed, as summed in the Table, the researchers was focusing on both lower and higher frequencies of terahertz spectrum to develop different antennas structures. However, all the assembled designs were marked by a narrow bandwidth, while some of them are limited by their low radiation efficiency. Hence, compared to the other previous works, the suggested antenna offers the widest bandwidth of about 1000 GHz with the highest radiation efficiency of 99.72%. Moreover, it provides a good comparable gain while preserving the most compact structure. As a result, all the mentioned traits allows the proposed antenna to be a suitable option for the wireless devices of terahertz applications.

**Fig. 13** 3D radiation pattern at 8 THz

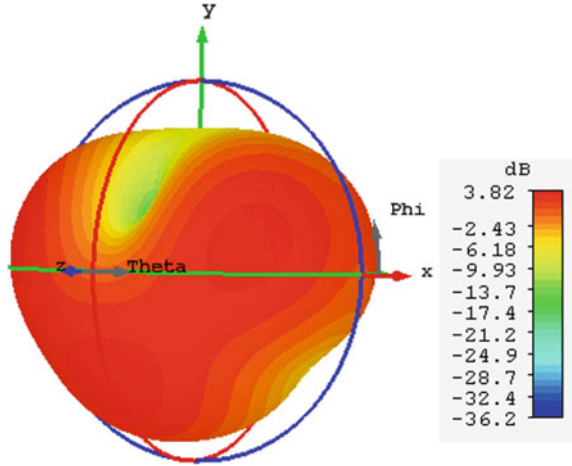
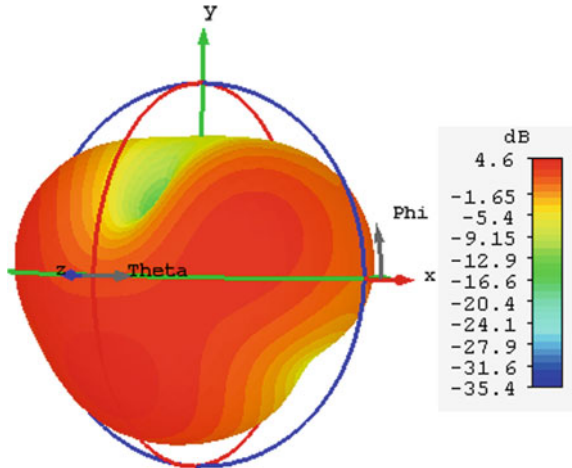


**Fig. 14** 3D radiation pattern at 8.15 THz



## 8 Conclusion

In this manuscript, an ultra-simple, ultra-wide band and super-tiny graphene-based annular ring antenna was developed and optimized for terahertz applications. The antenna was neatly designed using CST software to operate along a very wide terahertz spectrum range from 7.4 to 8.4 THz with high radiation efficiency reaches to 99.72% and maximum gain of 5 dB. The achieved results qualifies the proffered antenna to be a strong contender for terahertz wireless applications.

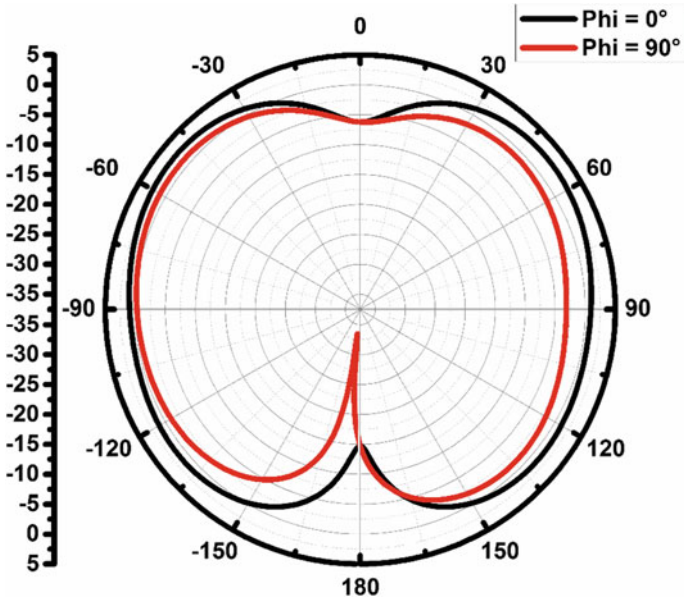


Fig. 15 Two dimension radiation pattern at 7.5 THz

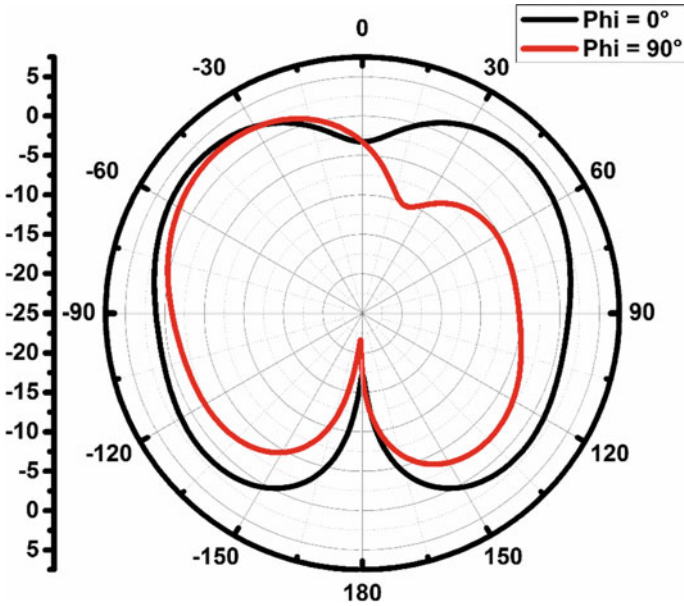


Fig. 16 Two dimension radiation pattern at 7 THz

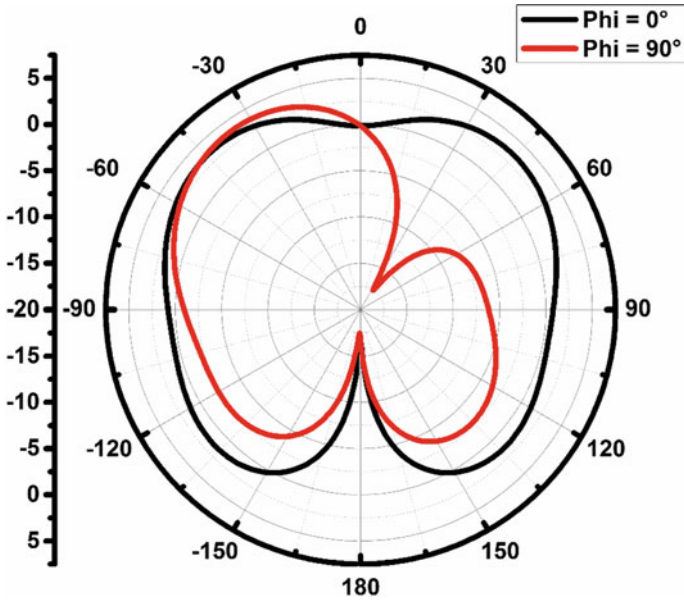


Fig. 17 Two dimension radiation pattern at 8 THz

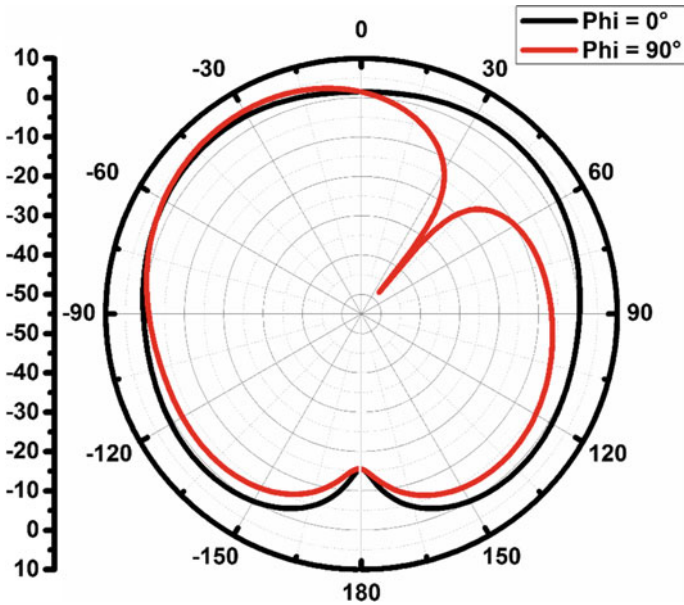


Fig. 18 Two dimension radiation pattern at 8.15 THz

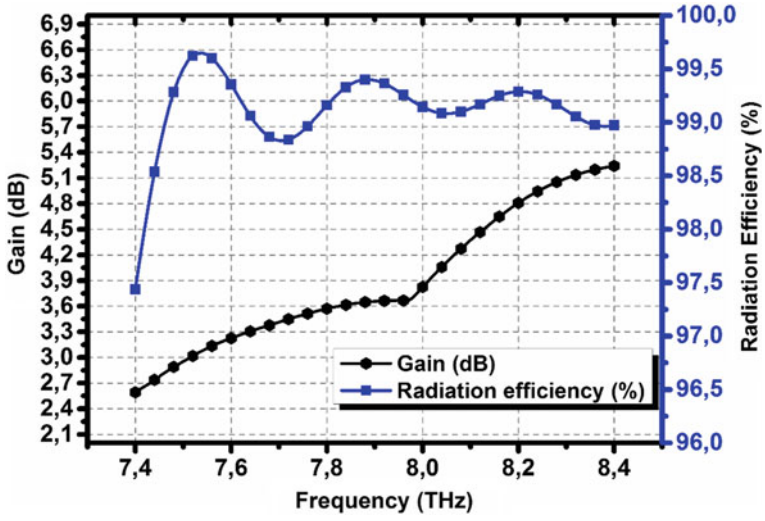


Fig. 19 Radiation efficiency and gain versus frequency

**Table 1** Comparison with other published works

References	Size ( $\mu\text{m}$ )	Substrate	Resonant frequency (THz)	Frequency range (THz)	Bandwidth (GHz)	Gain (dB)	Radiation efficiency (%)
[21]	$24 \times 24 \times 4.8$	Teflon ( $\epsilon_r = 2.1$ )	7	–	386	7.3	97.2
[23]	$120 \times 120 \times 45$	Arlon AD 1000 ( $\epsilon_r = 2.1$ )	0.72	0.57–0.84	270	–	–
[24]	$208 \times 422 \times 20$	Polyimide ( $\epsilon_r = 3.5$ )	0.67	0.65–0.69	40.16	5.22	–
[31]	$208 \times 433 \times 20$	Polyimide ( $\epsilon_r = 3.5$ )	0.75	0.725–0.775	50	5.09	86.58
[32]	$24 \times 24 \times 1.6$	Teflon ( $\epsilon_r = 2.1$ )	7.32	–	371	6.3	69.81
[33]	$28 \times 66.67 \times 2.5$	Polyimide ( $\epsilon_r = 3.5$ )	6.2	5.66–6.43	770	3.3	38.15
This work	$24 \times 24 \times 0.4$	Silicon ( $\epsilon_r = 11.9$ )	7.5 8.15	7.4–8.4	1000	5	99.72

## References

1. Xu, F., Lin, Y., Huang, J., Wu, D., Shi, H., Song, J., Li, Y.: Big data driven mobile traffic understanding and forecasting: a time series approach. *IEEE Trans. Serv. Comput.* **9**(5), 796–805 (2016)
2. Khabba, A., Wakrim, L., El Ouadi, Z., Amadid, J., Ibnyaich, S., Zeroual, A.: High gain double u-shaped slots microstrip patch antenna array for 28ghz 5g applications. In: 2022 International Conference on Decision Aid Sciences and Applications (DASA), pp. 1589–1592. IEEE (2022)
3. Khabba, A., Amadid, J., Ibnyaich, S., Zeroual, A.: Pretty-small four-port dual-wideband 28/38 ghz mimo antenna with robust isolation and high diversity performance for millimeter-wave 5g wireless systems. *Analog Integr. Circ. Sig. Process* **112**(1), 83–102 (2022)
4. Krishna, C.M., Das, S., Nella, A., Lakrit, S., Madhav, B.T.P.: A micro-sized rhombus-shaped thz antenna for high-speed short-range wireless communication applications. *Plasmonics* **16**(6), 2167–2177 (2021)
5. Khabba, A., Mohapatra, S., Wakrim, L., Ez-zaki, F., Ibnyaich, S., Zeroual, A.: Multiband antenna design with high gain and robust spherical coverage using a new 3d phased array structure for 5g mobile phone mm-wave applications. *Analog Integr. Circ. Sig. Process* **110**(2), 331–348 (2022)
6. Khabba, A., Amadid, J., Mohapatra, S., El Ouadi, Z., Ahmad, S., Ibnyaich, S., Zeroual, A.: Uwb dual-port self-decoupled o-shaped monopole mimo antenna with small-size easily extendable design and high diversity performance for millimeter-wave 5g applications. *Appl. Phys. A* **128**(8), 1–23 (2022)
7. Yang, P., Xiao, Y., Xiao, M., Li, S.: 6g wireless communications: Vision and potential techniques. *IEEE Netw.* **33**(4), 70–75 (2019)
8. Shafie, A., Yang, G.N., Han, C., Jornet, J.M., Juntti, M., Kurner, T.: Terahertz communications for 6g and beyond wireless networks: challenges, key advancements, and opportunities. *IEEE Netw.* (2022)
9. Huq, K.M.S, Rodriguez, J., Otung, I.E.: 3d network modeling for thzenabled ultra-fast dense networks: A 6g perspective. *IEEE Commun. Stand. Mag.* **5**(2), 84–90 (2021)
10. Yin, X.-X., Baghai-Wadji, A., Zhang, Y.: A biomedical perspective in terahertz nano-communications—a review. *IEEE Sens J* (2022)
11. Singh, M., Singh, S.: Design and performance investigation of miniaturized multi-wideband patch antenna for multiple terahertz applications. *Photonics Nanostruct. Fundam. Appl.* **44**, 100900 (2021)
12. Amin, M., Siddiqui, O., Abutarboush, H., Farhat, M., Ramzan, R.: thz graphene metasurface for polarization selective virus sensing. *Carbon* **176**, 580–591 (2021)
13. Dong, P., Liu, L., Li, S., Hu, S., Bu, L.: Application of m5 model tree in passive remote sensing of thin ice cloud microphysical properties in terahertz region. *Remote Sens* **13**(13), 2569 (2021)
14. Li, H., Li, C., Wu, S., Zheng, S., Fang, G.: Adaptive 3d imaging for moving targets based on a simo inisar imaging system in 0.2 Thz band. *Remote Sens.* **13**(4), 782 (2021)
15. Abdullah-Al-Shafi, M., Akter, N., Sen, S., Hossain, M.S.: Design and performance analysis of background material of zeonex based high core power fraction and extremely low effective material loss of photonic crystal fiber in the terahertz (thz) wave pulse for many types of communication areas. *Optik* **243**, 167519 (2021)
16. Hasan, M.M., Pandey, T., Habib, M.A.: Highly sensitive hollow-core fiber for spectroscopic sensing applications. *Sens. Bio-Sens. Res.* **34**, 100456 (2021)
17. Khaleel, S.A., KI Hamad, E., Parchin, N.O., Saleh, M.B.: Mtm-inspired graphene-based thz mimo antenna configurations using characteristic mode analysis for 6g/iot applications. *Electronics* **11**(14), 2152 (2022)
18. Tassin, P., Koschny, T., Soukoulis, C.M.: Graphene for terahertz applications. *Science* **341**(6146), 620–621 (2013)
19. Nissiyah, G.J., Madhan, M.G.: Graphene based microstrip antenna for triple and quad band operation at terahertz frequencies. *Optik* **231**, 166360 (2021)

20. Nissiyah, G.J., Madhan, M.G.: Graphene-based photoconductive antenna structures for directional terahertz emission. *Plasmonics* **14**(4), 891–900 (2019)
21. Khan, M., Kaium, A., Ullah, M., Kabir, R., Alim, M.A., et al.: High-performance graphene patch antenna with superstrate cover for terahertz band application. *Plasmonics* **15**(6), 1719–1727 (2020)
22. Nissiyah, G.J., Madhan, M.G.: A narrow spectrum terahertz emitter based on graphene photoconductive antenna. *Plasmonics* **14**(6), 2003–2011 (2019)
23. Shamim, S., Uddin, M.S., Hasan, M., Samad, M., et al.: Design and implementation of miniaturized wideband microstrip patch antenna for high-speed terahertz applications. *J. Comput. Electron.* **20**(1), 604–610 (2021)
24. Dhillon, A.S., Mittal, D., Sidhu, E.: Thz rectangular microstrip patch antenna employing polyimide substrate for video rate imaging and homeland defence applications. *Optik* **144**, 634–641 (2017)
25. Kushwaha, R.K., Karuppanan, P., Malviya, L.D.: Design and analysis of novel microstrip patch antenna on photonic crystal in thz. *Physica B Condens. Matter* **545**, 07–112 (2018)
26. Tang, W.X., Zhang, H.C., Ma, H.F., Jiang, W.X., Cui, T.J.: Concept, theory, design, and applications of spoof surface plasmon polaritons at microwave frequencies. *Adv. Opt. Mater.* **7**(1), 1800421 (2019)
27. Wang, Y., Liu, H., Wang, S., Cai, M., Ma, L.: Optical transport properties of graphene surface plasmon polaritons in mid-infrared band. *Curr. Comput.-Aided Drug Des.* **9**(7), 354 (2019)
28. Dash, S., Patnaik, A.: Impact of silicon-based substrates on graphene thz antenna. *Phys. E.* **126**, 114479 (2021)
29. Aloui, R., Zairi, H., Mira, F., Llamas-Garro, I., Mhatli, S.: Terahertz antenna based on graphene material for breast tumor detection. *Sens. Bio-Sens. Res.* 100511 (2022)
30. Cao, M., Xiong, D.-B., Yang, L., Li, S., Xie, Y., Guo, Q., Li, Z., Adams, H., Gu, J., Fan, T., et al.: Ultrahigh electrical conductivity of graphene embedded in metals. *Adv. Funct. Mater.* **29**(17), 1806792 (2019)
31. Anand, S., Kumar, D.S., Wu, R.J., Chavali, M.: Graphene nanoribbon based terahertz antenna on polyimide substrate. *Optik* **125**(19), 5546–5549 (2014)
32. Khan, M.A.K., Shaem, T.A., Alim, M.A.: Graphene patch antennas with different substrate shapes and materials. *Optik* **202**, 163700 (2020)
33. Thampy, A.S., Darak, M.S., Dhamodharan, S.K.: Analysis of graphene based optically transparent patch antenna for terahertz communications. *Phys. E Lowdimensional Syst. Nanostruct.* **66**, 67–73 (2015)